Supplemental Material

© Copyright 2022 American Meteorological Society (AMS)
For permission to reuse any portion of this work, please contact permissions@ametsoc.org. Any use of material in this work that is determined to be “fair use” under Section 107 of the U.S. Copyright Act (17 USC §107) or that satisfies the conditions specified in Section 108 of the U.S. Copyright Act (17 USC §108) does not require AMS’s permission. Republication, systematic reproduction, posting in electronic form, such as on a website or in a searchable database, or other uses of this material, except as exempted by the above statement, requires written permission or a license from AMS. All AMS journals and monograph publications are registered with the Copyright Clearance Center (https://www.copyright.com). Additional details are provided in the AMS Copyright Policy statement, available on the AMS website (https://www.ametsoc.org/PUBSCopyrightPolicy).

Support information

Uncertainty in the winter tropospheric response to Arctic Sea ice loss: the role of stratospheric polar vortex internal variability

Lantao Sun*

Department of Atmospheric Science, Colorado State University,

Fort Collins, CO

Clara Deser and Isla Simpson

National Center for Atmospheric Research Climate & Global Dynamics,

Boulder, CO

Michael Sigmond

Canadian Centre for Climate Modelling and Analysis, Victoria, British

Columbia, Canada.

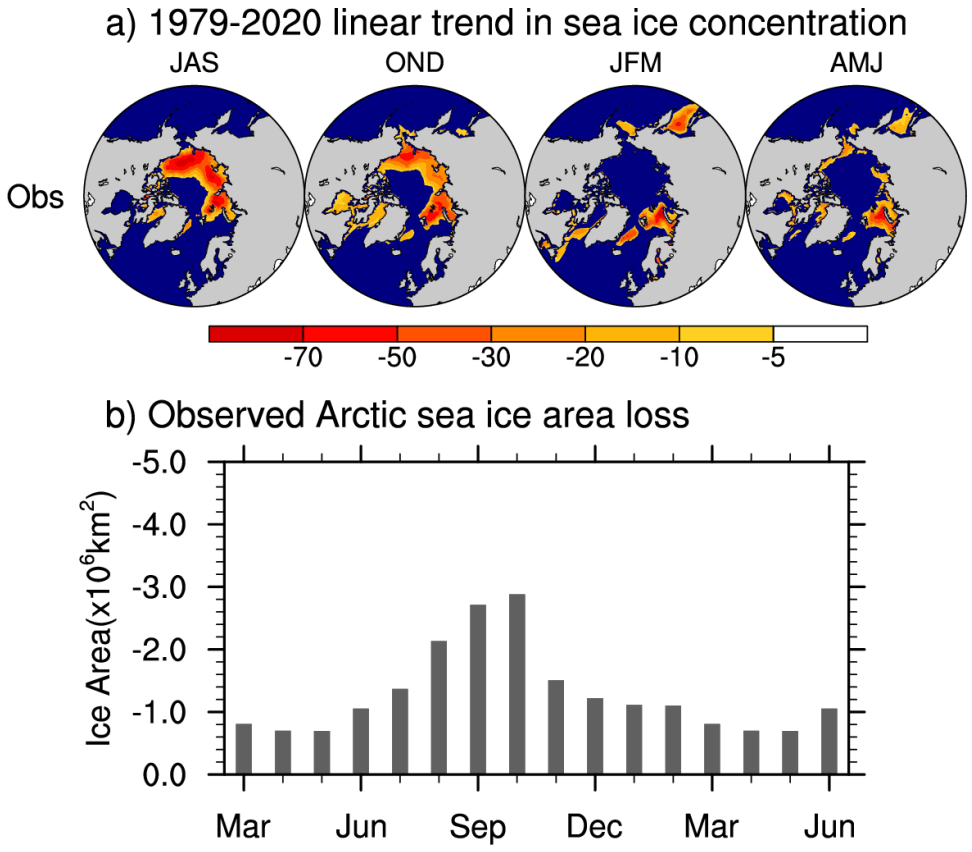

Figure S1. (a) Seasonal maps of 1979-2020 linear trend in sea ice concentration (%) based on merged Hadley-Optimum Interpolation (OI) SIC (Had-OI; Hurrell et al. 2008) data updated through 2020. Summer, autumn, winter and spring seasons are defined to be the average of July-September (JAS), October-December (OND), January-March (JFM) and April-June (AMJ), respectively. (b) Observed Arctic sea ice area loss (10^6 km^2) during 1979-2020; note the inverted y-axis scale.

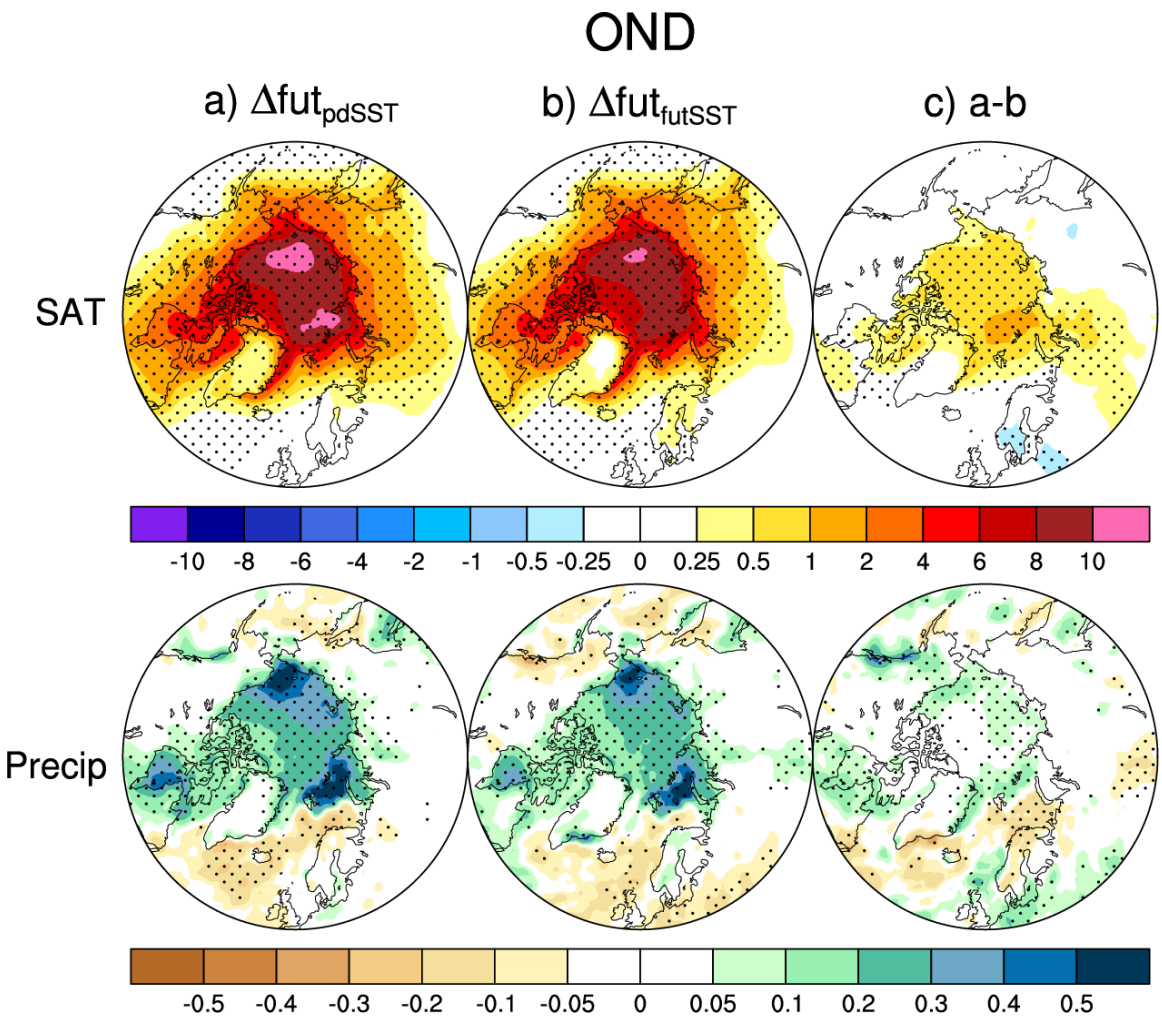

Figure S2. OND atmospheric response to future Arctic sea ice loss for: (a) Δfut_{pdSST}; Δfut_{futSST} and (c) their difference. Two rows indicate (from top to bottom): SAT (shading; ^{o}C) and precipitation (shading; mm day^{-1}). Stippling indicates the 90% statistical significance based on a two-sided student's t-test and false discovery rate (FDR; Wilks 2016).

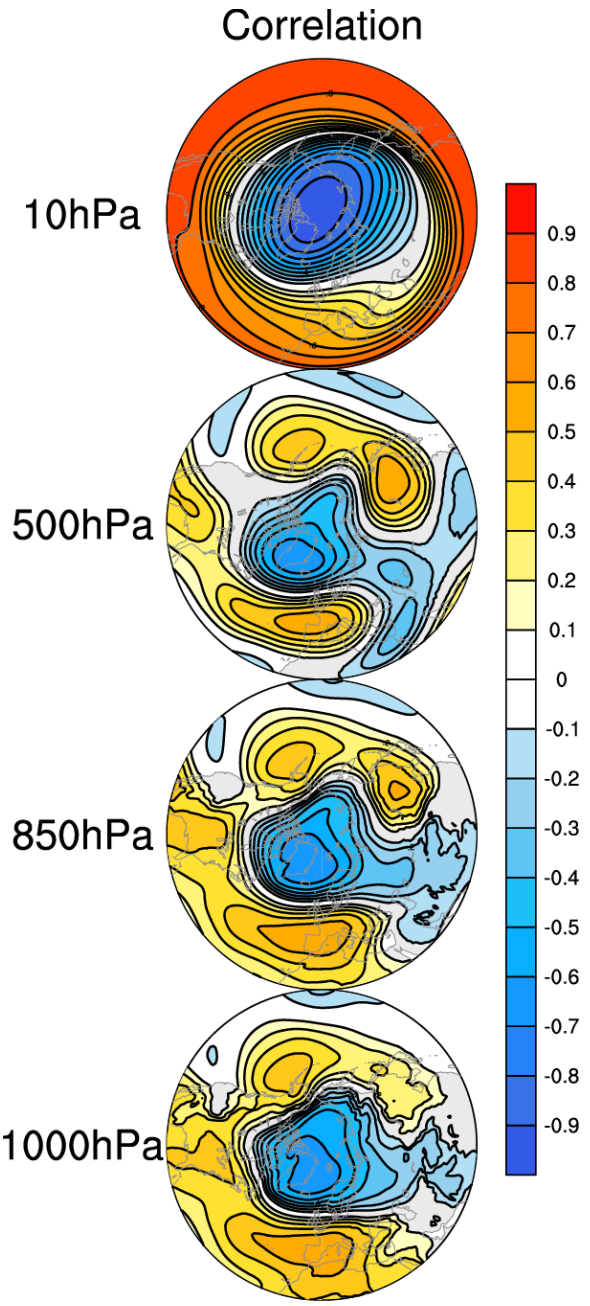

Figure S3. Correlation of geopotential height response with U10 across the 1000 bootstrapped samples of 100-member averages. Rows 1-4 show the correlation of 10 hPa DJF response and the 500-hPa, 850-hPa and 1000-hPa response in JFM, respectively.

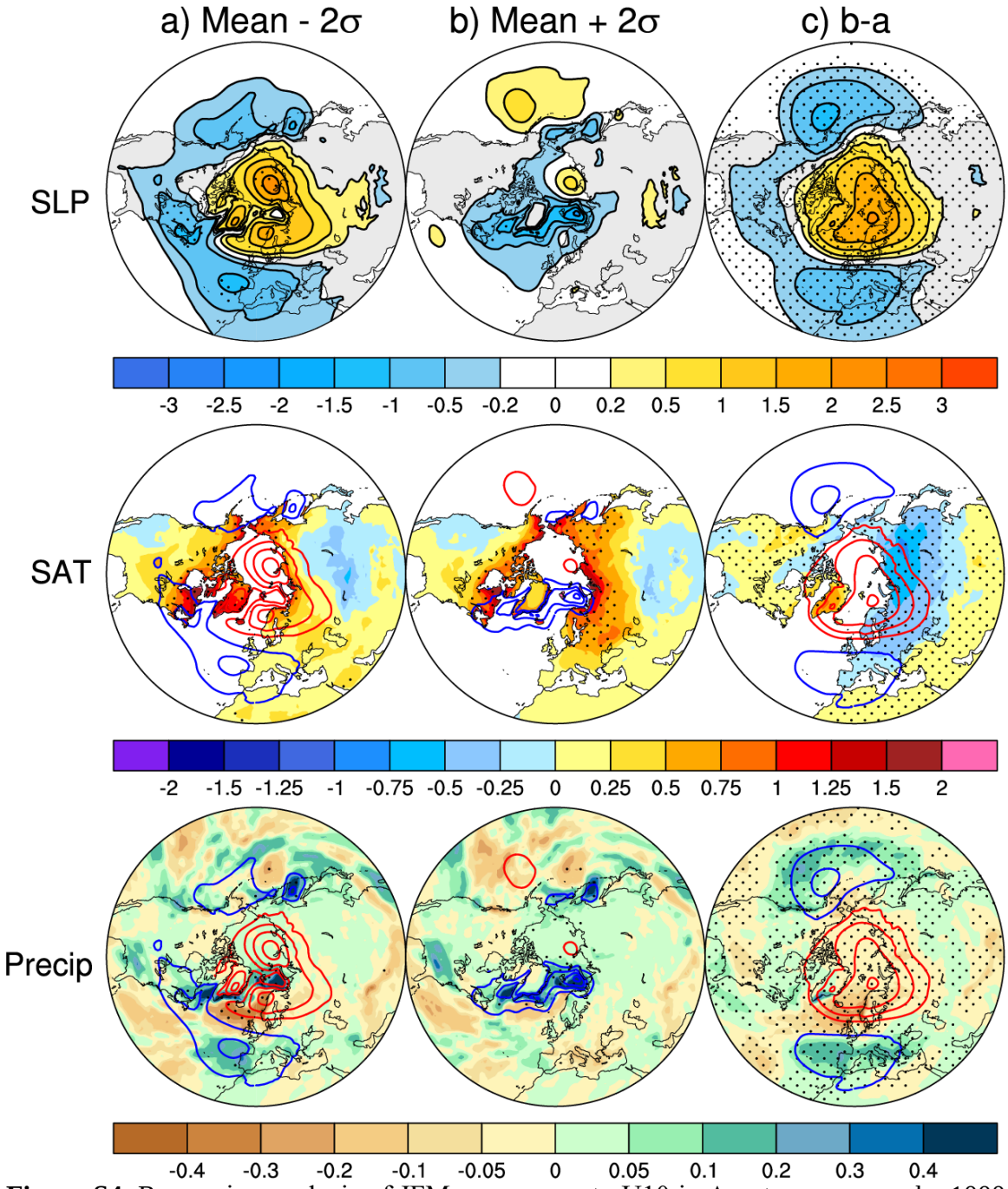

Figure S4. Regression analysis of JFM response onto U10 in $\Delta past_{pdSST}$ across the 1000 bootstrapped samples of 100-member averages. Rows 1-3 show the SLP (shading; hPa), SAT (shading; ^{o}C) and precipitation (shading; mm day^{-1}) responses, respectively. Panels a, b and c show the Mean-2σ, Mean+2σ and their difference, respectively. The SLP responses (contours; interval of 0.5 hPa) are overlaid on the SAT and precipitation panels. Red and blue contours denote positive and negative values, respectively. Zero contour line has been omitted. Stippling indicates the 90% statistical significance based on a two-sided student's t-test and false discovery rate.

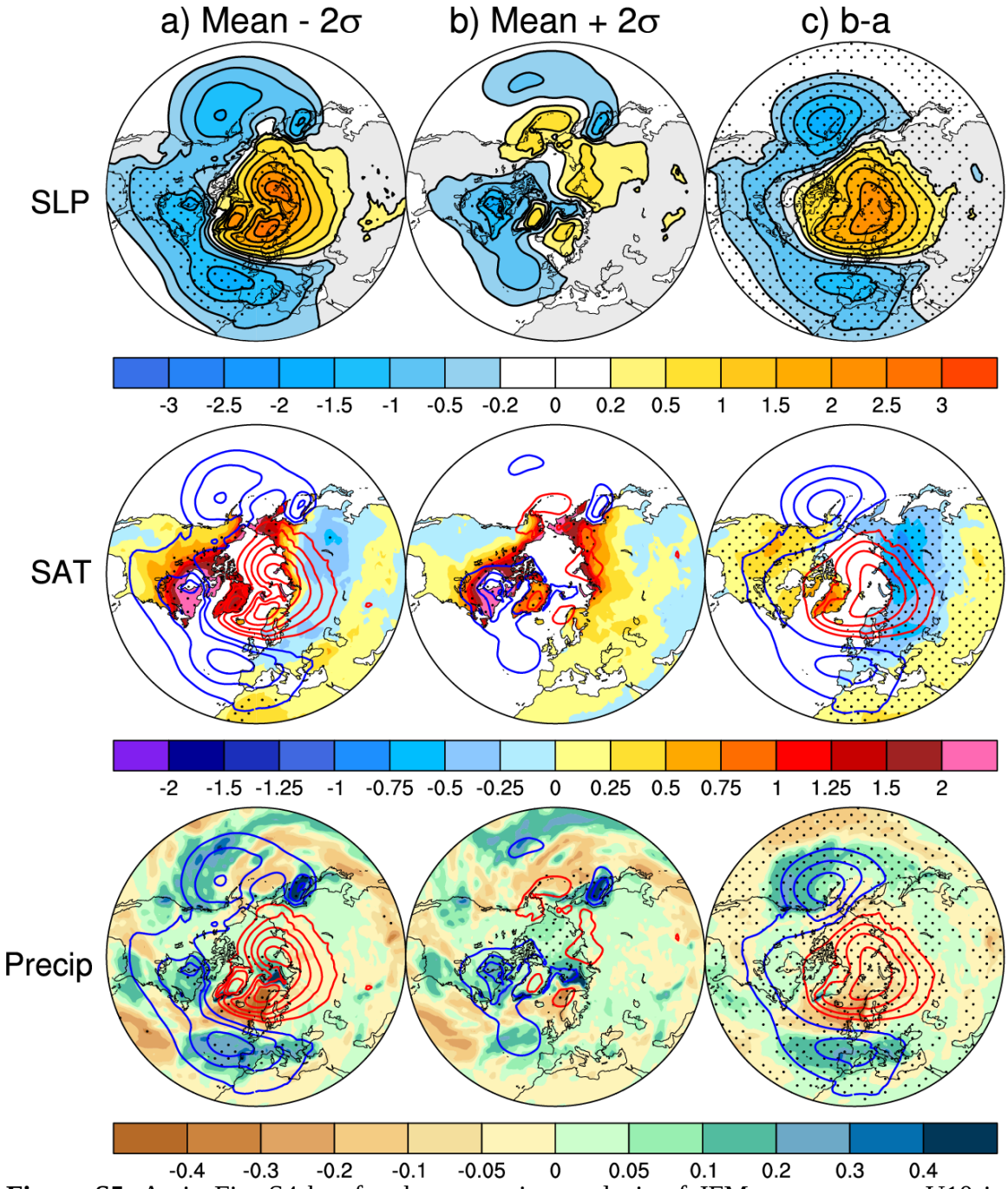

Figure S5. As in Fig. S4 but for the regression analysis of JFM response onto U10 in Δfut_{futSST} across the 1000 bootstrapped samples.

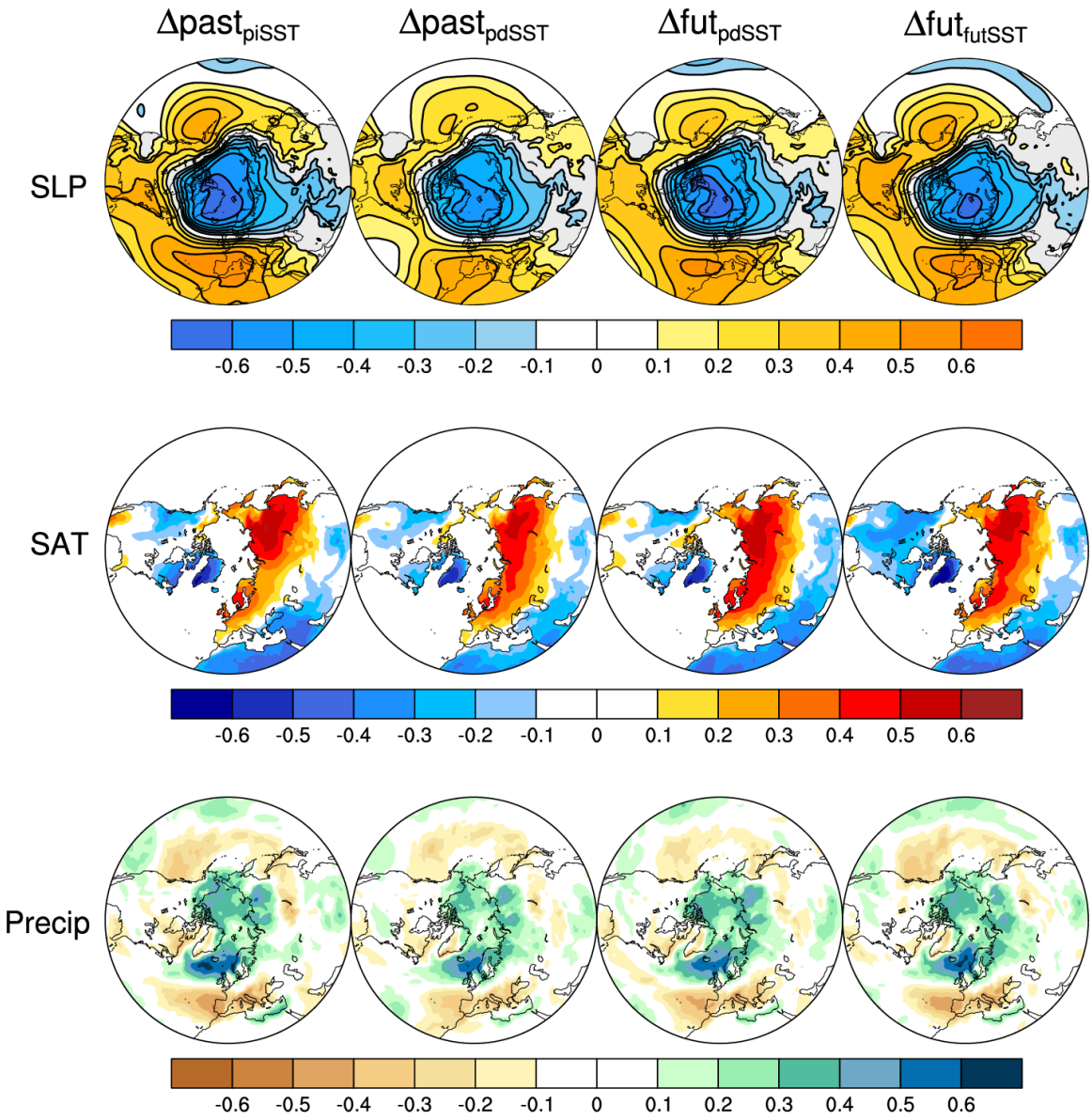

Figure S6. Correlation of JFM (from top to bottom) SLP, SAT and precipitation responses with U10 across the 1000 bootstrapped samples for (from left to right): $\Delta past_{piSST}$; $\Delta past_{pdSST}$; Δfut_{pdSST} and Δfut_{futSST}.

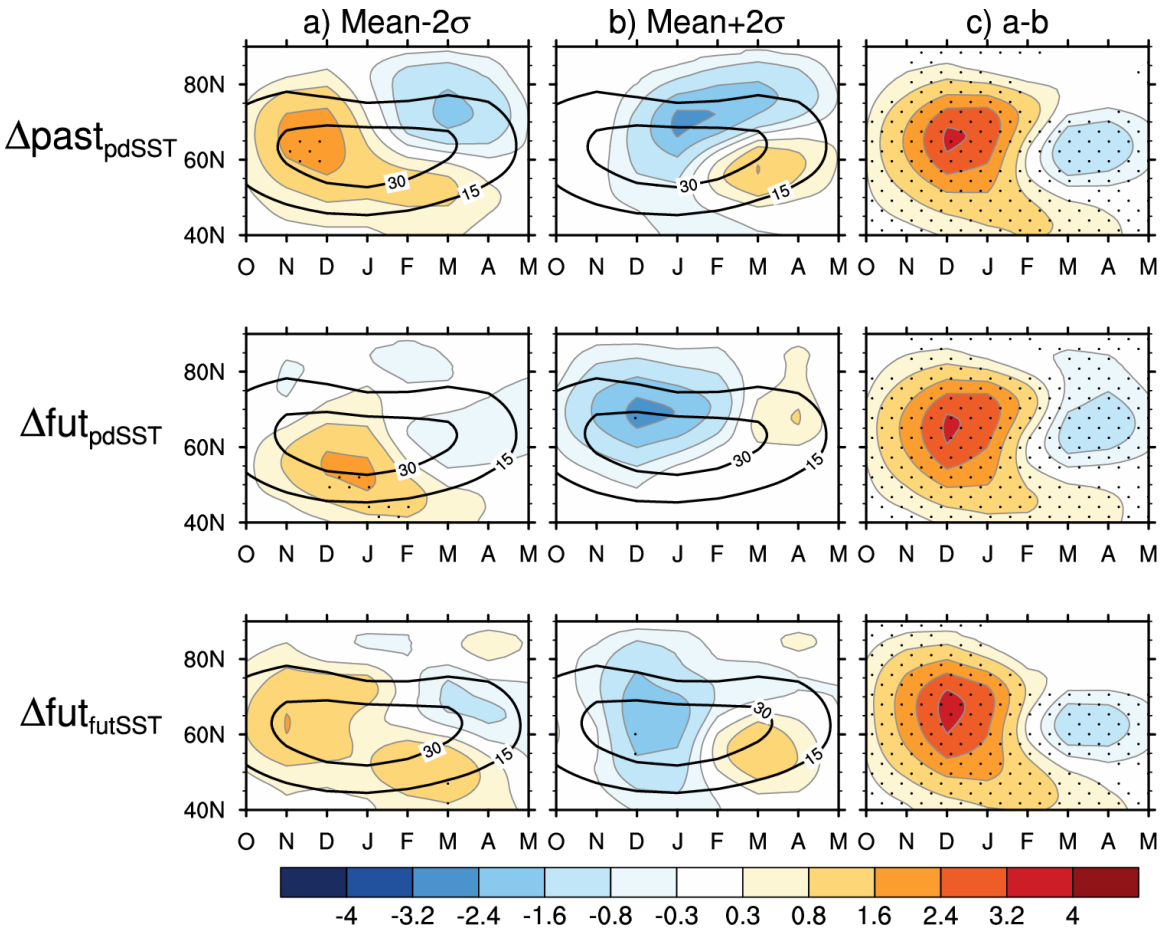

Figure S7. Regression analysis of eddy heat flux response onto U10 across the 1000 bootstrapped samples of 100-member averages for (from top to bottom): $\Delta past_{pdSST}$; Δfut_{pdSST} and Δfut_{futSST}. Panels a, b and c show the Mean-2σ, Mean+2σ and their difference, respectively. Stippling indicates the 90% statistical significance based on a two-sided student's t-test and false discovery rate. The climatologies (contours; interval of 15 K m s^{-1}) are overlaid on the panels a and b.

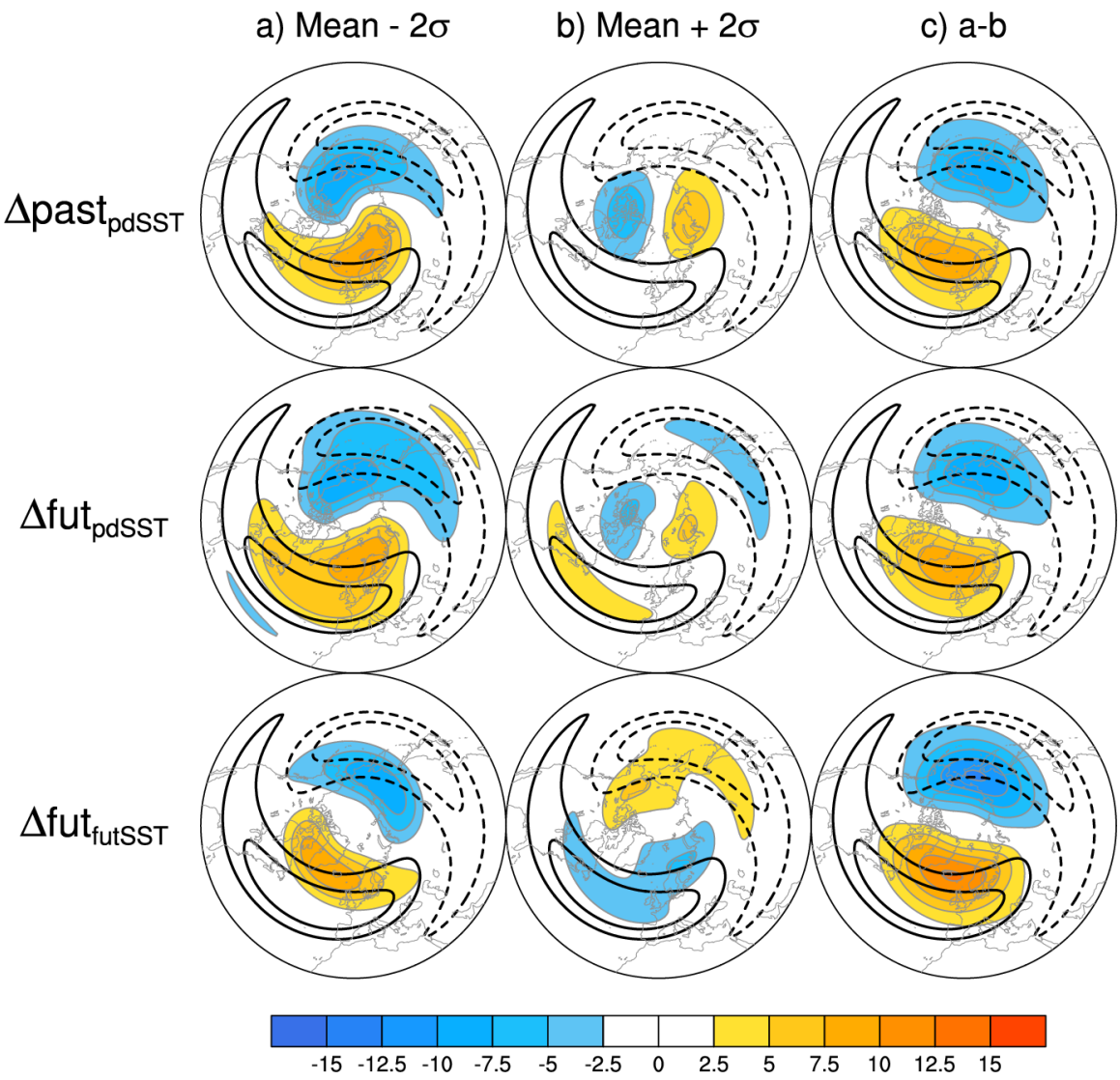

Figure S8. Regression analysis of NDJ zonal wave-1 response at 300 hPa onto U10 in across the 1000 bootstrapped samples for (from top to bottom): $\Delta past_{pdSST}$; Δfut_{pdSST} and Δfut_{futSST}. Panels a, b and c show the Mean-2σ, Mean+2σ and their difference, respectively. The climatologies (contours; interval of 50 m) are overlaid on the panels a, b and c. solid and dashed contours denote positive and negative values, respectively. Zero contour line has been omitted.

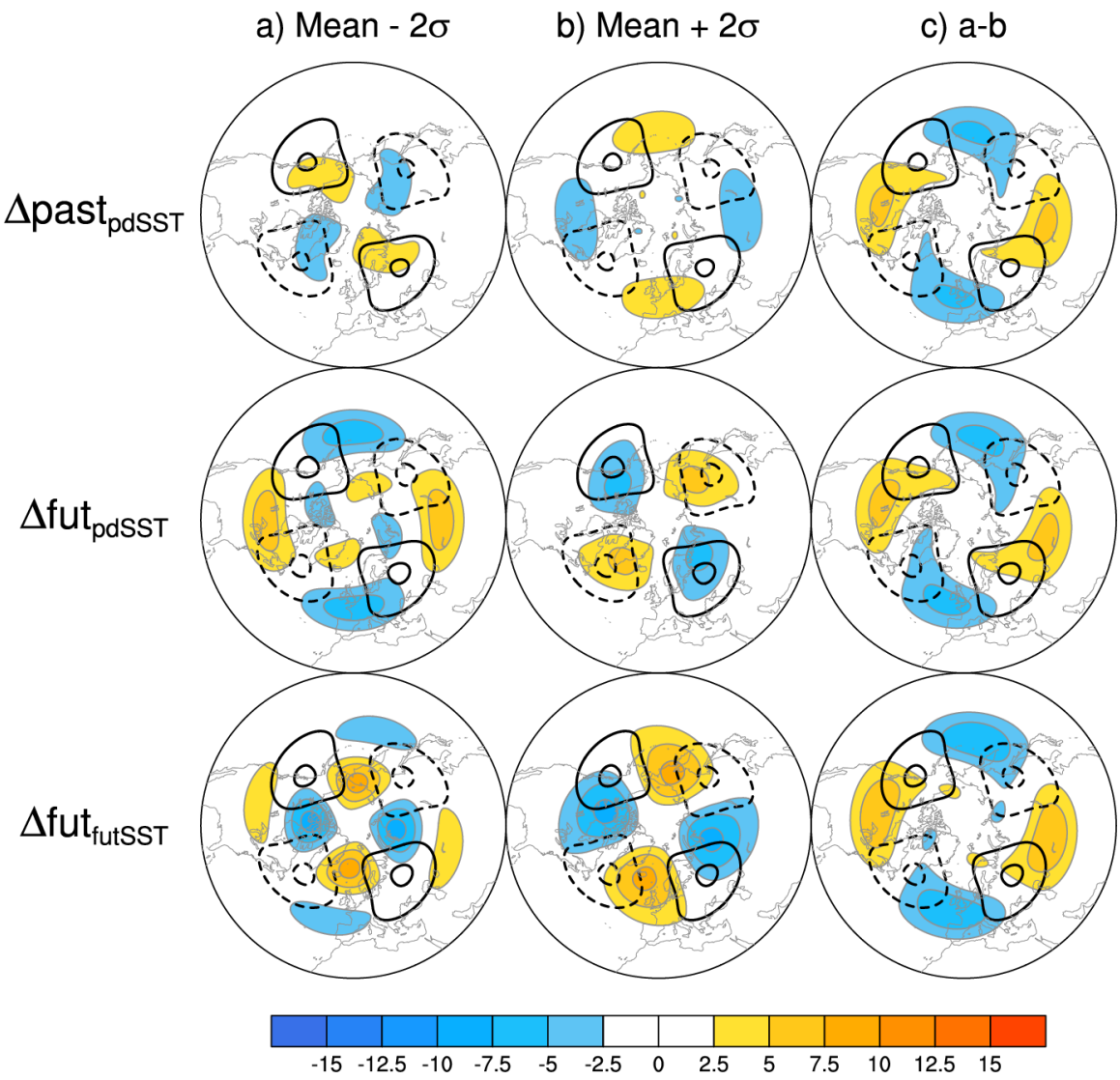

Figure S9. As in Fig. S8, but for the regression analysis of NDJ zonal wave-2 response at 300 hPa onto U10 in across the 1000 bootstrapped samples.

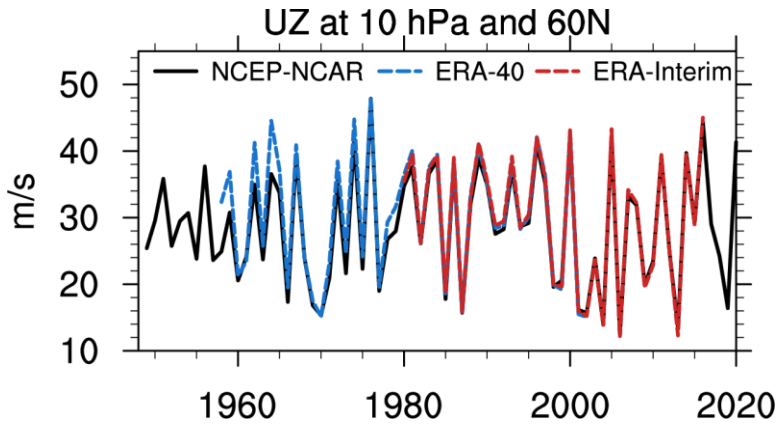

Figure S10. Time series of zonal-mean zonal wind at 10 hPa and 60°N based on the NCEP-NCAR reanalysis (solid black curve), ERA-40 (dashed blue curve) and ERA-Interim (dashed red curve) datasets.

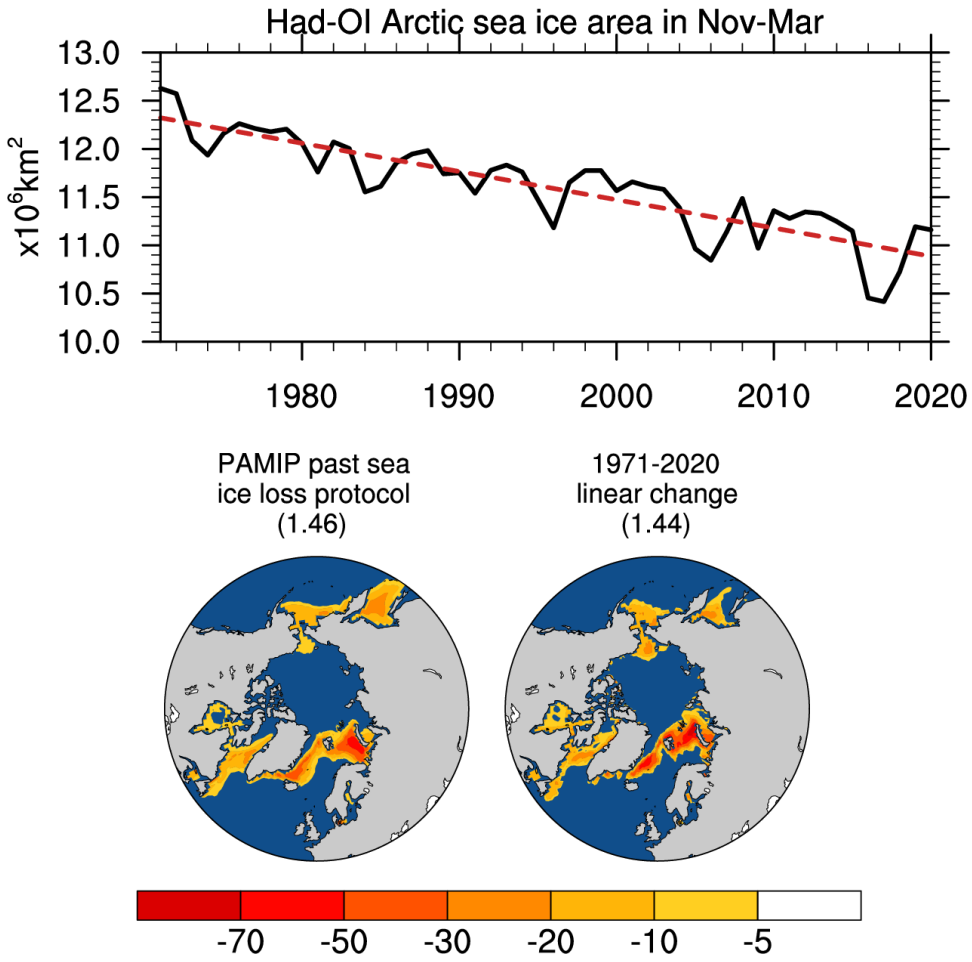

Figure S11. (Top) Arctic sea ice area time series in November-March based on merged Hadley-Optimum Interpolation (OI) sea ice concentration (Had-OI; Hurrell et al. 2008) (black curve) and its linear trend (red dashed line) during 1971-2020. (Bottom) November-March averaged Arctic SIC loss (%) in the PAMIP past sea ice loss protocol (left) and observed linear change during 1971-2020. The numbers on the parentheses indicate the corresponding Arctic sea ice area loss (10^6 km^2).

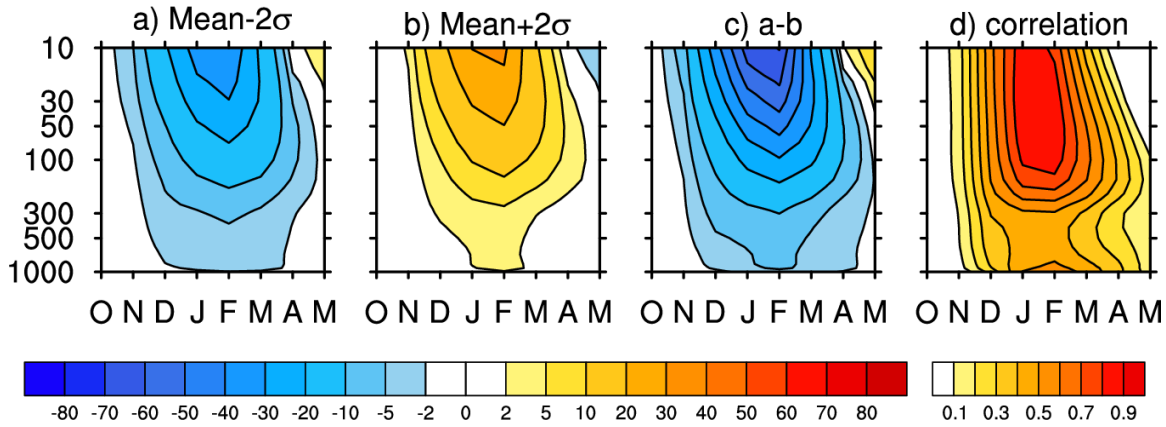

Figure S12. Regression analysis of 60°N zonal-mean zonal wind response in $\Delta past_{piSST}$ onto U10 (defined as DJF zonal-mean zonal wind at 10 hPa and 60°N) across the 1000 bootstrapped samples of single ensemble members. Panels a, b and c show the Mean-2σ, Mean+2σ and their difference, respectively. Panel d shows the correlation of the zonal-mean zonal wind response with U10 across the 1000 bootstrapped samples.

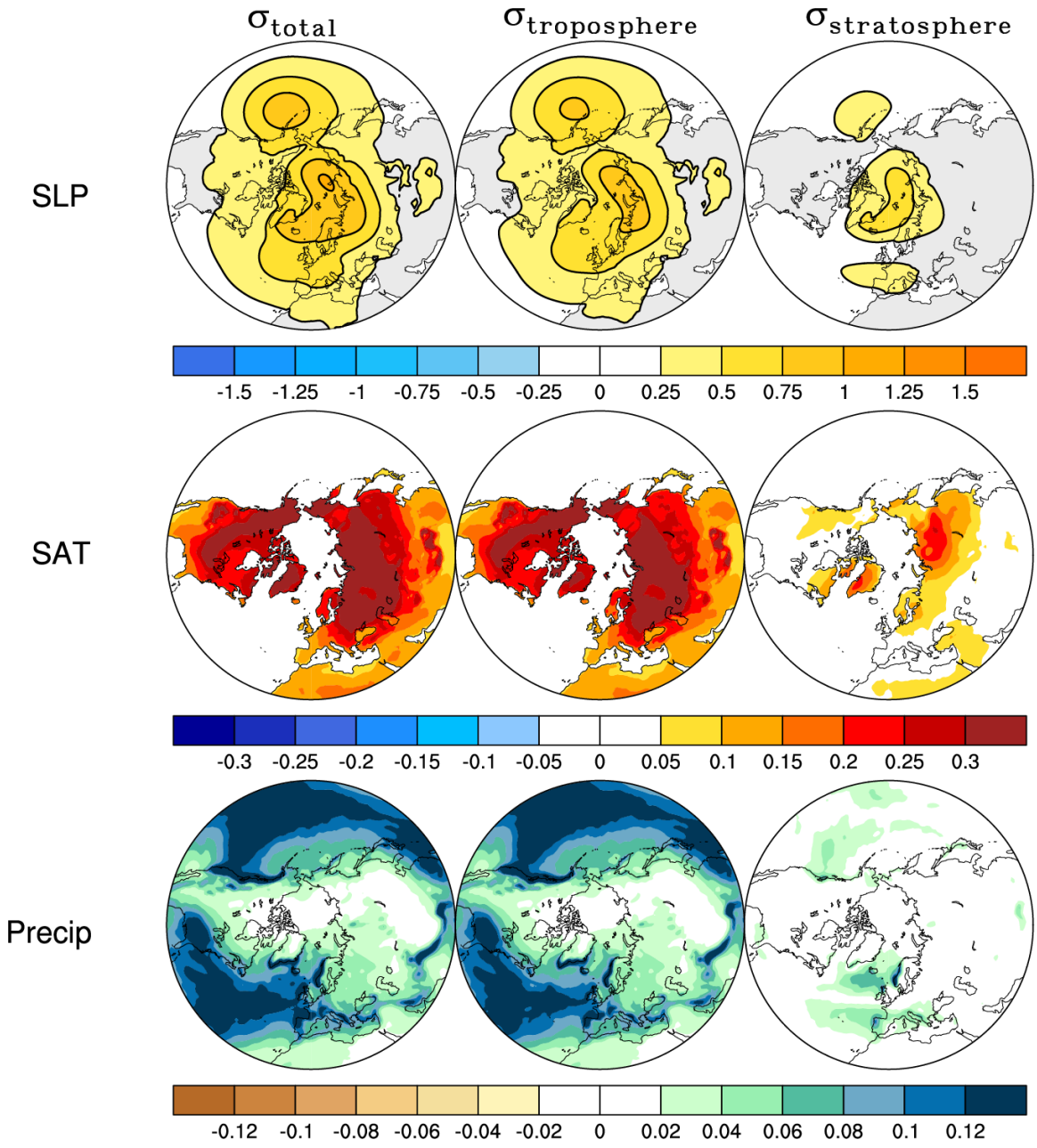

Figure S13. Standard deviation of JFM response in $\Delta past_{piSST}$ across the 1000 bootstrapped samples of 100-member averages for (from top to bottom): SLP (shading; hPa), SAT (shading; ^{o}C) and precipitation (shading; mm day^{-1}). Column 1-3 show the total standard deviation (σ_{total}), standard deviation after removing the component that is linearly related to U10 ($\sigma_{troposphere}$; similar to Simpson et al. 2018), and the standard deviation that is linearly related to U10 ($\sigma_{stratosphere} = \sqrt{{\sigma_{total}}^2 - {\sigma_{troposphere}}^2}$), respectively.

REFERENES

Hurrell, James W., James J. Hack, Dennis Shea, Julie M. Caron, James Rosinski (2008), A New Sea Surface Temperature and Sea Ice Boundary Dataset for the Community Atmosphere Model. *J. Climate*, 21, 5145–5153. doi: 0.1175/2008JCLI2292.1.

Simpson, I. R., Hitchcock, P., Seager, R., Wu, Y., & Callaghan, P. (2018). The Downward Influence of Uncertainty in the Northern Hemisphere Stratospheric Polar Vortex Response to Climate Change, *Journal of Climate*, 31(16), 6371-6391. Retrieved Jul 9, 2021, from https://journals.ametsoc.org/view/journals/clim/31/16/jcli-d-18-0041.1.xml